

## FULL PAPER

# Analysis of Various Manipulator Configurations Based on Multi-Objective Black-Box Optimization

Kento Kawaharazuka<sup>a\*</sup>, Keita Yoneda<sup>a</sup>, Takahiro Hattori<sup>a</sup>, Shintaro Inoue<sup>a</sup>, and Kei Okada<sup>a</sup>

<sup>a</sup>*The Department of Mechano-Informatics, Graduate School of Information Science and Technology, The University of Tokyo, 7-3-1 Hongo, Bunkyo-ku, Tokyo, Japan.*

(Received 00 Month 201X; accepted 00 Month 201X)

This is a preprint of an article whose final and definitive form has been published in ADVANCED ROBOTICS 2025, copyright Taylor & Francis and Robotics Society of Japan, is available online at: <http://www.tandfonline.com/Article DOI>; <https://doi.org/10.1080/01691864.2025.2607670>.

Various 6-degree-of-freedom (DOF) and 7-DOF manipulators have been developed to date. Over a long history, their joint configurations and link length ratios have been determined empirically. In recent years, the development of robotic foundation models has become increasingly active, leading to the continuous proposal of various manipulators to support these models. However, none of these manipulators share exactly the same structure, as the order of joints and the ratio of link lengths differ among robots. Therefore, in order to discuss the optimal structure of a manipulator, we performed multi-objective optimization from the perspectives of end-effector reachability and joint torque. We analyze where existing manipulator structures stand within the sampling results of the optimization and provide insights for future manipulator design.

**Keywords:** Black-Box Optimization, Manipulator, Design Optimization

## 1. Introduction

A wide range of 6-degree-of-freedom (DOF) and 7-DOF manipulators have been developed over the years. These manipulators have a long history, beginning with the development of Unimate [1], the world's first industrial manipulator, in 1961. Since then, many manipulators have been proposed, leading up to today's ALOHA [2] for robotic foundation models [3–5]. Unimate has joints arranged in the order of YPSPY (where Roll is denoted as R, Pitch as P, Yaw as Y, and Slide as S, and the sequence is described from the base of the manipulator. The initial state of a serial manipulator is defined as the configuration in which all links are extended vertically upward, and the joint types (R, P, Y, S) are determined based on the direction of movement in this state.) Although some robots have been developed using slide joints, most subsequent general-purpose manipulators have been composed of Roll, Pitch, and Yaw joints. Among 6-DOF manipulators, ALOHA [2], COBOTTA [6], and xArm 6 [7] have joints arranged in the order of YPPYPY. Additionally, the ARX [8] used in the recent  $\pi_0$  [9] has a joint order of YPPPRY, while myCobot [10] follows the order of YPPPYR. For 7-DOF manipulators, Franka Emika Panda [11] has a joint order of YPYPYPR, while Sawyer [12] and Kinova Gen3 [13] have joints arranged in the order of YPYPYPY. As seen above, the order of joints in manipulators varies from robot to robot, and the ratio of link lengths also differs accordingly.

The structure of manipulators has traditionally been determined empirically. However, as various manipulator configurations continue to be developed, numerous studies have focused on optimizing body structure design to determine the most effective configurations. In [14], an optimal joint configuration

---

\*Corresponding author. Email: [kawaharazuka@jsk.imi.i.u-tokyo.ac.jp](mailto:kawaharazuka@jsk.imi.i.u-tokyo.ac.jp)

## Sampling Results of Multi-Objective Black-Box Optimization

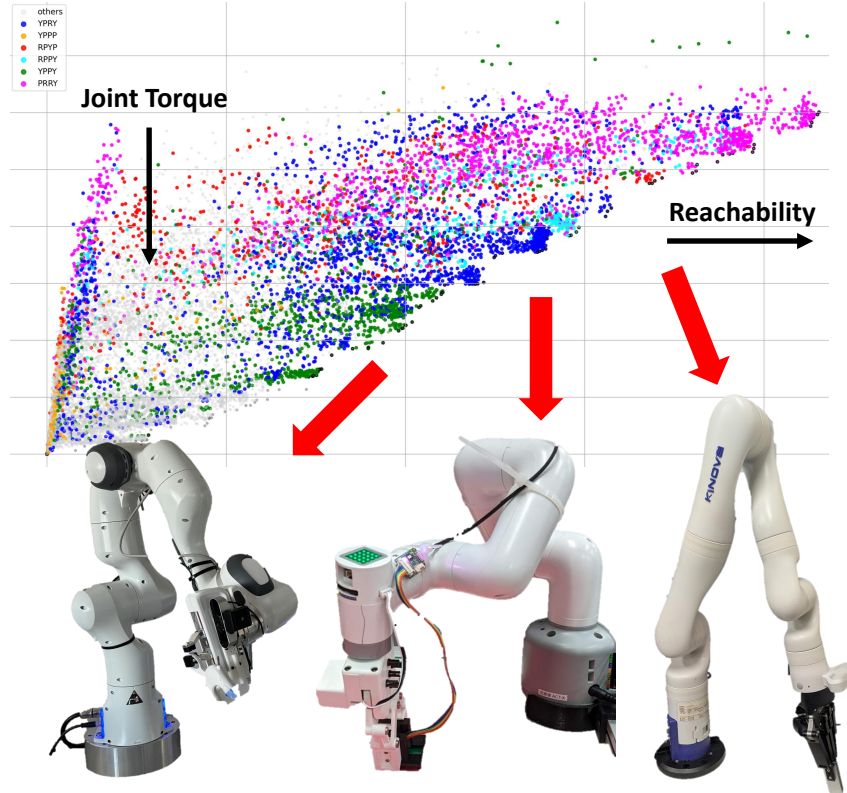


Figure 1. Research concept: By performing multi-objective optimization from the perspectives of end-effector reachability and joint torque, this study discusses various joint structures, including the diverse manipulators that have been actively developed in recent years.

for a 6-DOF manipulator was proposed based on workspace maximization and the concept of a well-connected workspace. In [15], heuristic methods were used to extract several joint configurations for a 7-DOF manipulator, which were then evaluated based on singularity avoidance, workspace optimization, kinematic simplicity, and mechanical feasibility. For industrial robots, [16] optimized the number and types of modules, as well as their relative positions, using a genetic algorithm to satisfy desired task points. In [17], a multi-objective optimization of motor and gear ratios for a 6-DOF manipulator was performed using a genetic algorithm, aiming to minimize body weight while maximizing manipulability. In [18], an exhaustive search was conducted to optimize the design of modular robots capable of executing tasks while satisfying constraints such as joint angle limits, torque limits, and collision avoidance. In [19], an evolutionary strategy was used to optimize module placement to minimize required torque and maximize manipulability while following a commanded trajectory. Furthermore, [20, 21] proposed a Pareto-optimal solution for minimizing control error and required torque through multi-objective optimization using a genetic algorithm, enabling body structure adaptation based on tasks and user preferences.

These studies can be categorized based on different approaches. For example, there are studies utilizing analytical optimization [14, 15] and black-box optimization [16–20]. Additionally, there are studies focused on evaluating task-independent universal performance [14, 15] and those that perform task-specific optimization [16–20]. Historically, analytical methods were used to optimize task-independent performance [14, 15]. On the other hand, recent research has increasingly focused on performing more complex and multi-objective optimizations tailored to specific tasks using black-box optimization methods [16–20]. Analytical optimization have limitations, such as the inability to account for joint angle limits and link collisions. Also, they only focus on reachability, without considering multi-objective optimization which includes joint torque. In contrast, modern black-box optimization methods enable the consideration of multiple constraints and multi-objective optimization. However, most of these studies focus on task-specific optimization, and there has been little effort to perform a unified multi-objective

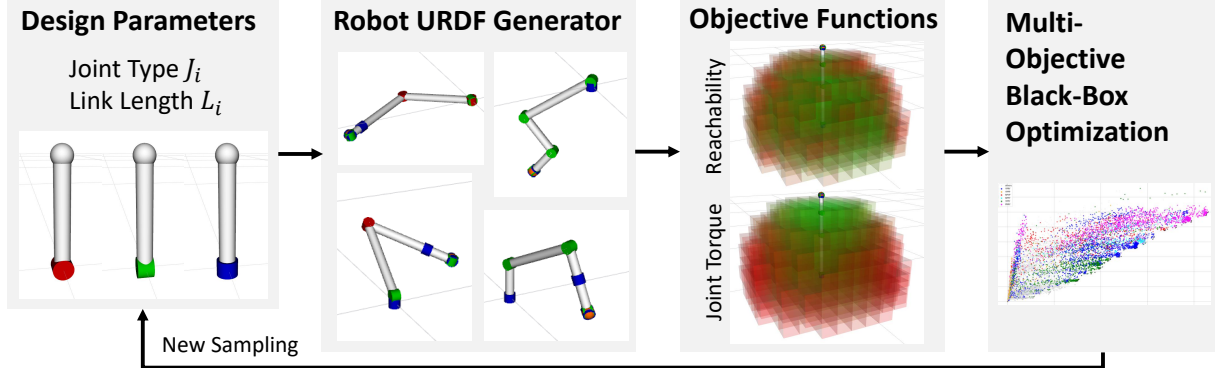


Figure 2. System overview: This study parametrizes joint types and link lengths, automatically generates URDFs, and performs multi-objective optimization from the perspectives of end-effector reachability and joint torque to discuss the structures of various manipulators.

optimization of general manipulator structures, providing a comprehensive discussion of the diverse manipulator structures currently being developed.

To address this gap, this study performs a multi-objective optimization of general 6-DOF and 7-DOF manipulators from the perspectives of end-effector reachability and joint torque, analyzing various manipulator structures comprehensively (Fig. 1). The optimization considers discrete joint types and continuous link lengths as parameters, applying certain constraints and using a Tree-Structured Parzen Estimator (TPE) [22] for multi-objective optimization. This approach clarifies the position of existing manipulator structures within the optimization sampling and provides insights for future manipulator design.

The remainder of this paper is structured as follows. Section 2 describes the design parameters, constraints, objective functions, and details of the multi-objective optimization used in this study. Section 3 presents the results of the multi-objective optimization for 6-DOF and 7-DOF manipulators and discusses the findings based on the sampling results for currently developed manipulators. Section 4 provides further discussion of the study's results, and conclusions are presented in Section 5.

## 2. Design of Various Manipulator Configurations Based on Multi-Objective Black-Box Optimization

The overall framework of this study is shown in Fig. 2. First, the design parameters for joint types and link lengths are determined. Second, individual joints described as xacro (XML macro) files are combined to automatically generate the robot's URDF (Unified Robot Description Format). Finally, the objective functions – end-effector reachability and joint torque – are computed, and multi-objective optimization is performed based on these criteria.

### 2.1 Design Parameters of Manipulators

The design parameters considered in this study are described in Fig. 3. Here, the origin of the manipulator coincides with the origin of the workspace. Additionally, in the initial posture where all joint angles are set to 0, the manipulator extends straight upward in the vertical direction. The types of joint angles are determined based on this initial posture.

For an  $N_{joint}$ -DOF manipulator, the joint types and link lengths are treated as design parameters. Each joint  $J_i$  ( $1 \leq i \leq N_{joint}$ ) is selected from three types: Roll, Pitch, and Yaw. The link length  $L_i$  ( $1 \leq i \leq N_{joint}$ ) is represented as a value within the range  $[0, L^{max}]$ . The URDF of the manipulator is constructed by including the xacro files of each joint. Each joint's xacro file contains parameters such as the link length following that joint, motor mass, and link mass. The motor mass is denoted as  $m_{motor}$ , while the link mass is expressed as  $\pi r^2 L_i \rho$ , where  $r$  represents the link radius and  $\rho$  denotes the link density. Furthermore, the joint angle limits for all joints are set within the range  $[-\frac{3}{4}\pi, \frac{3}{4}\pi]$ .

Several constraints are imposed on these design parameters. First, consecutive Yaw joints are not

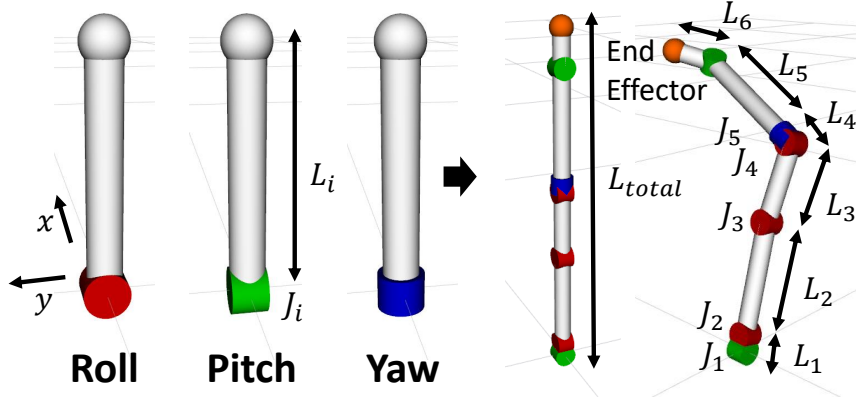


Figure 3. Design parameters handled in this study: The joint type  $J_i$  and link length  $L_i$  are varied as design parameters.

allowed, as having a Yaw joint followed by another Yaw joint is redundant. Next, a Roll or Pitch joint following a Yaw joint can achieve the same motion by rotating the Yaw joint. Therefore, these cases are unified into Pitch joints. In summary, if  $J_i$  is a Yaw joint, then  $J_{i+1}$  must be a Pitch joint. Additionally, the total link length, i.e., the overall length of the manipulator, is fixed at  $L_{total}$ . The specific implementation of these constraints is discussed in Section 2.3.

## 2.2 Objective Functions of Reachability and Joint Torque

The objective functions used in the optimization process of this study are described below. Here, a multi-objective optimization is performed based on two criteria: end-effector reachability [23] and joint torque (Fig. 4). Of course, it is possible to consider additional perspectives, but due to the difficulty of visualizing them and the fact that the evaluation function defined in this study – based on position and force – is the most general-purpose, the optimization is conducted with respect to these two aspects.

First, the workspace for evaluation is defined as follows.

$$x \in [x^{\min}, x^{\max}], \quad y \in [y^{\min}, y^{\max}], \quad z \in [z^{\min}, z^{\max}] \quad (1)$$

This workspace is uniformly voxelized with an interval of  $d_{voxel}$ , and the set of all voxels is denoted as  $\mathcal{V}$ . For each voxel  $i \in \mathcal{V}$ , let  $p_i$  be the center position of that voxel. Additionally, for each voxel  $i$ ,  $N_{rand}$  random end-effector postures are generated, and inverse kinematics is solved while changing the posture at position  $p_i$ . The success rate of the inverse kinematics solution is defined as the reachability score  $E_i^{reach}$  and is formulated as follows,

$$E_i^{reach} = \frac{\sum_{j=1}^{N_{rand}} S_{ij}}{N_{rand}} \quad (2)$$

where  $S_{ij} = 1$  if the inverse kinematics problem is successfully solved for the  $j$ -th random posture in voxel  $i$ , and  $S_{ij} = 0$  otherwise. The inverse kinematics algorithm used follows the methods proposed in [24, 25], which also account for joint angle limits and collision detection between links. Due to the dependence on initial conditions, if the inverse kinematics solution fails, it is retried up to  $N_{ik} = 5$  times with random initial joint angles. Additionally, for each voxel  $i$ , the norm of the average required joint torque  $E_i^{torque}$  for successful inverse kinematics solutions is computed as follows,

$$E_i^{torque} = \frac{1}{\sum_{j=1}^{N_{rand}} S_{ij}} \sum_{j=1}^{N_{rand}} S_{ij} \|\boldsymbol{\tau}_{ij}\| \quad (3)$$

where  $\boldsymbol{\tau}_{ij} \in \mathbb{R}^{N_{joint}}$  is the joint torque vector required for the  $j$ -th solution in voxel  $i$ , and  $\|\cdot\|$  represents

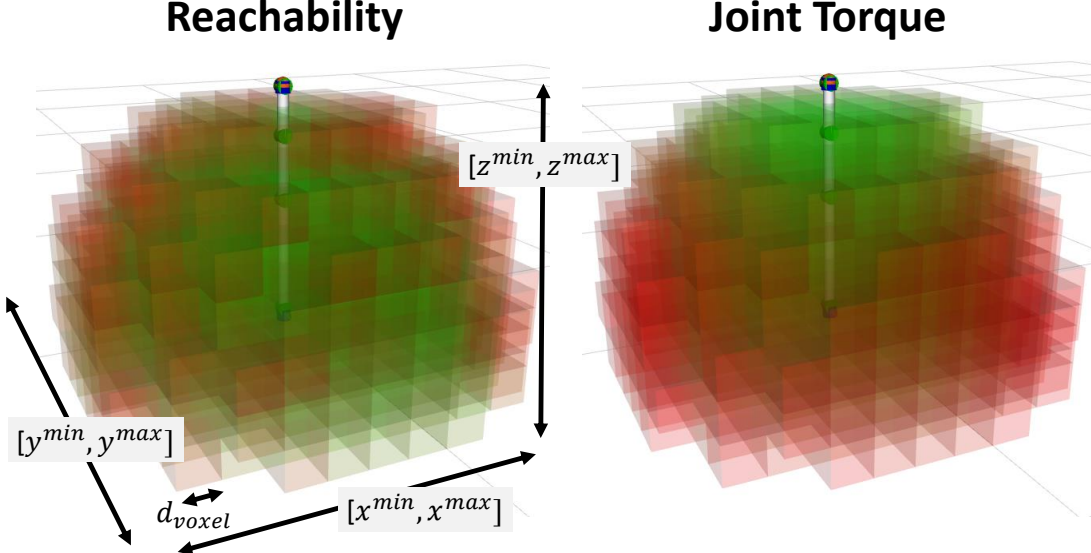


Figure 4. Objective functions for multi-objective optimization: The left image shows end-effector reachability, while the right image shows necessary joint torque.

the L2 norm. Finally, the overall reachability and joint torque scores across the entire workspace are computed as follows.

$$E^{reach} = \sum_{i \in \mathcal{V}} E_i^{reach}, \quad E^{torque} = \sum_{i \in \mathcal{V}} E_i^{torque} \quad (4)$$

For example, Fig. 4 illustrates the reachability and joint torque distribution for a manipulator with a YPPYP joint structure. The parameters were set as follows:  $x^{\min} = -0.5, x^{\max} = 0.5, y^{\min} = -0.5, y^{\max} = 0.5, z^{\min} = -0.1, z^{\max} = 0.5, d_{voxel} = 0.1$ , and  $N_{rand} = 30$ . For each voxel in the visualization, reachability is represented with red for  $E_i^{reach} = 0$  and green for  $E_i^{reach} = 1$ . Also, joint torque is represented with green for  $E_i^{torque} = 3.0 \text{ Nm}$  and red for  $E_i^{torque} = 10.0 \text{ Nm}$  (this visualization approach will also be used in subsequent experiments). In this example, reachability is higher near the origin and decreases as the distance from the origin increases. Additionally, joint torque decreases as the manipulator extends in the  $z$ -direction and increases as it extends in the  $x$ - or  $y$ -direction.

### 2.3 Multi-Objective Black-Box Optimization

Based on the previously described design parameters and objective functions, multi-objective optimization is performed. For the multi-objective optimization, the Tree-Structured Parzen Estimator (TPE) [22] is used. Specifically, the multivariate TPE [26], which considers dependencies between parameters, is employed. This enables the discovery of various design solutions from the sampling results.

Here,  $J_i$  is treated as a categorical variable with three choices, while  $L_i$  is treated as a continuous variable. The optimization is performed based on maximizing  $E^{reach}$  and minimizing  $E^{torque}$ . During this process, the constraints described in Section 2.1 must be considered. First, to enforce the rule that a Pitch joint follows a Yaw joint, when  $J_i$  is Yaw,  $J_{i+1}$  is set to Pitch regardless of which choice is selected. This is due to the limitation in the optuna [27] implementation, where categorical variable choices cannot be dynamically modified. Next, since the total link length is fixed at  $L_{total}$ ,  $L^{max}$  is dynamically adjusted regarding  $L_i$ . For  $i = 1$ ,  $L^{max}$  is set as  $L^{max} = L_{init}^{max}$  (where  $L_{init}^{max}$  is a constant). For  $i > 1$ ,  $L^{max}$  is updated

dynamically as follows.

$$L_i^{remain} = L_{total} - \sum_{j=1}^{i-1} L_j \quad (5)$$

$$L_i^{max} = \min(L_{init}^{max}, L_i^{remain}) \quad (6)$$

Furthermore, to ensure the total link length remains  $L_{total}$ , the final link length is set as  $L_{N_{joint}} = L_{N_{joint}}^{remain}$ . Thus, the actual parameters optimized are  $J_i$  ( $1 \leq i \leq N_{joint}$ ) and  $L_i$  ( $1 \leq i \leq N_{joint} - 1$ ). For other parameters, the number of initial random trials for multi-objective optimization is set to  $N_{init}^{trial} = 100$ , and the total number of optimization trials is set to  $N_{total}^{trial} = 20000$ .

### 3. Experiments

The experimental setup of this study is described below. First, two experiments are conducted by varying the number of joints as  $N_{joint} = \{6, 7\}$ . For the parameters related to the objective function calculation, the following values are used considering generality and computational cost:  $x^{\min} = -0.5, x^{\max} = 0.5, y^{\min} = -0.5, y^{\max} = 0.5, z^{\min} = -0.1, z^{\max} = 0.5, d_{voxel} = 0.2$ , and  $N_{rand} = 30$ . For other parameters, the following values are set considering general manipulator configurations:  $m_{motor} = 0.5$  kg,  $\rho = 1.0 \times 10^3$  kg/m<sup>3</sup>,  $r = 0.015$  m,  $L_{total} = 0.6$  m, and  $L_{init}^{max} = 0.3$  m. For each experiment, the sampling results from the multi-objective optimization are presented, and several structural examples are discussed in detail.

#### 3.1 Multi-Objective Optimization of 6-DOF Manipulator

The experimental results for  $N_{joint} = 6$  are shown in Fig. 5. In the sampling results, different colors represent variations in the first four joint configurations. Pareto-optimal solutions are highlighted with black circular frames. The six main configurations observed were **PRRY**, **RPYP**, **YPRY**, **RPPY**, **YPPY**, and **YPPP**. Among these, the joint configurations with the highest reachability within the Pareto-optimal solutions (**PRRY**, **RPYP**, and **YPRY**) are illustrated in the lower figure of Fig. 5. Additionally, the joint configurations with the highest reachability among the sampled non-Pareto-optimal solutions (**YPPY** and **YPPP**) are also presented. Since **RPPY** is nearly identical to **PRRY** due to symmetry along the  $x$ - and  $y$ -axes, it is omitted.

A general trend observed is that, even within the same joint structure, increasing reachability often results in placing two DOFs near the origin (shoulder), one Pitch or Roll joint at the intermediate position (elbow), and three DOFs at the end-effector (wrist). This finding is consistent with what was reported in [14].

The specific joint configurations are discussed below. **PRRY** exhibits both high overall reachability and low required torque. In particular, **PRRY** has low torque around the  $y$ -axis, while **RPPY** has low torque around the  $x$ -axis. **RPYP** places the Yaw joint in the middle, allowing the end-effector to achieve various postures. However, its reachability is reduced in positions close to the body. This structure reflects a conflict between two motives, resulting in an indecisive configuration. One aims to determine the 3D orientation with the initial RPY and place a Pitch joint in the middle. The other seeks to allocate all three RPY degrees of freedom to the end-effector. **YPPY** has two consecutive Pitch joints after a Yaw joint, making it susceptible to gravitational effects. However, its overall reachability remains quite high. This configuration is used in manipulators such as ALOHA, COBOTTA, and xArm 6. Manipulators mounted on quadruped robot platforms like Boston Dynamics' Spot [28] also share this structure. **YPPP** is the configuration adopted by ARX and myCobot. Similar to **YPPY**, it is directly influenced by gravitational effects. With three consecutive Pitch joints, its reachability is relatively low, but it offers the simplest and most intuitive kinematics.

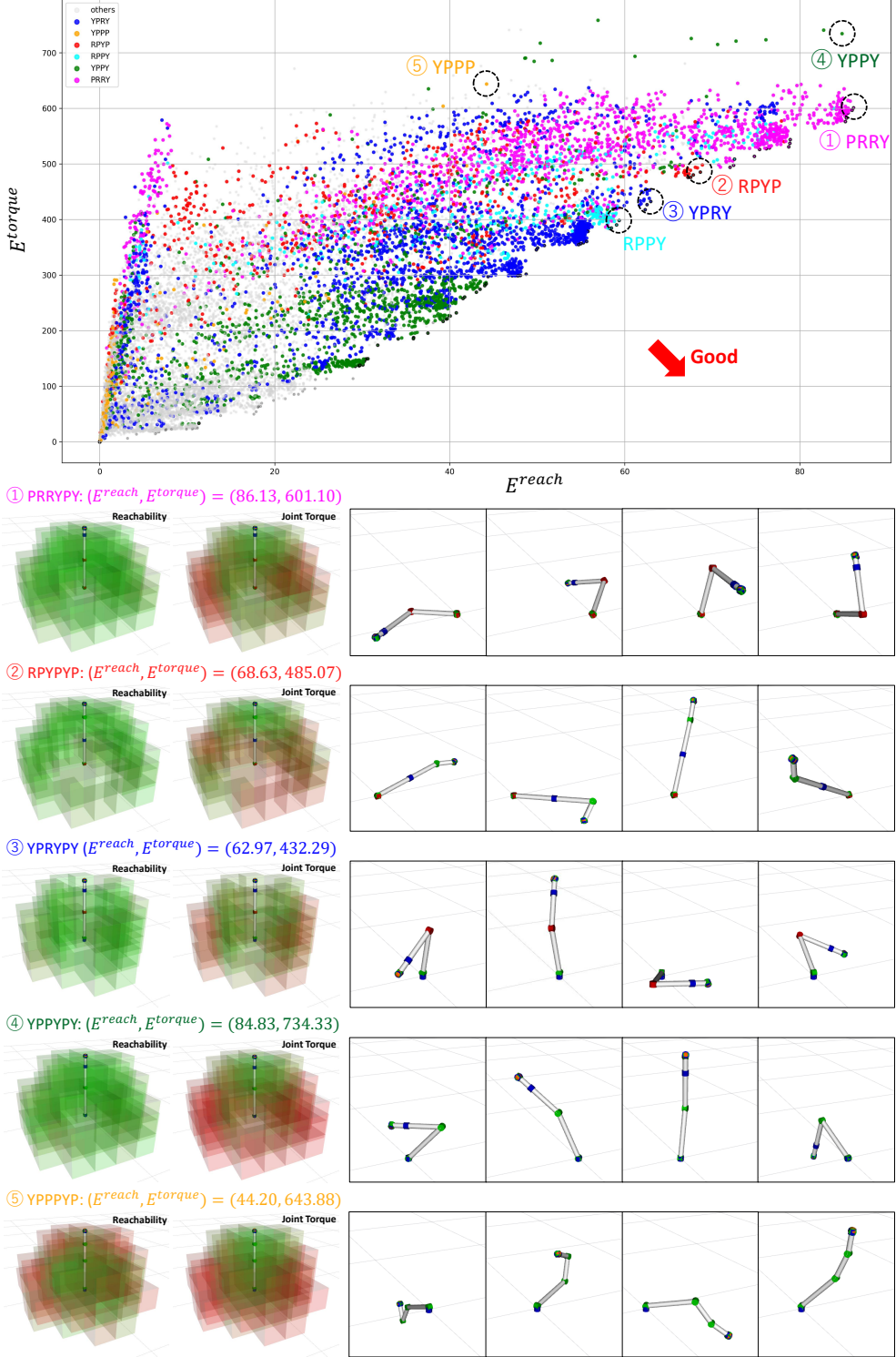


Figure 5. Optimization results for a 6-DOF manipulator: The upper figure visualizes the sampling results, color-coded based on differences in the first four joint types. The lower figure presents a subset of the solutions, showing end-effector reachability, joint torque, and four postures generated by assigning random joint angles.

### 3.2 Multi-Objective Optimization of 7-DOF Manipulator

The experimental results for  $N_{joint} = 7$  are shown in Fig. 6. The main joint configurations observed were **PRRY**, **YPRR**, **YPRY**, **YPPP**, **YPPY**, **YPYP**, and **YPRP**. Note that the color assignments for the joint configurations may differ between the 6-DOF and 7-DOF cases. Among these, the joint configurations with the highest reachability within the Pareto-optimal solutions (**PRRY** and **YPRP**) are illustrated in

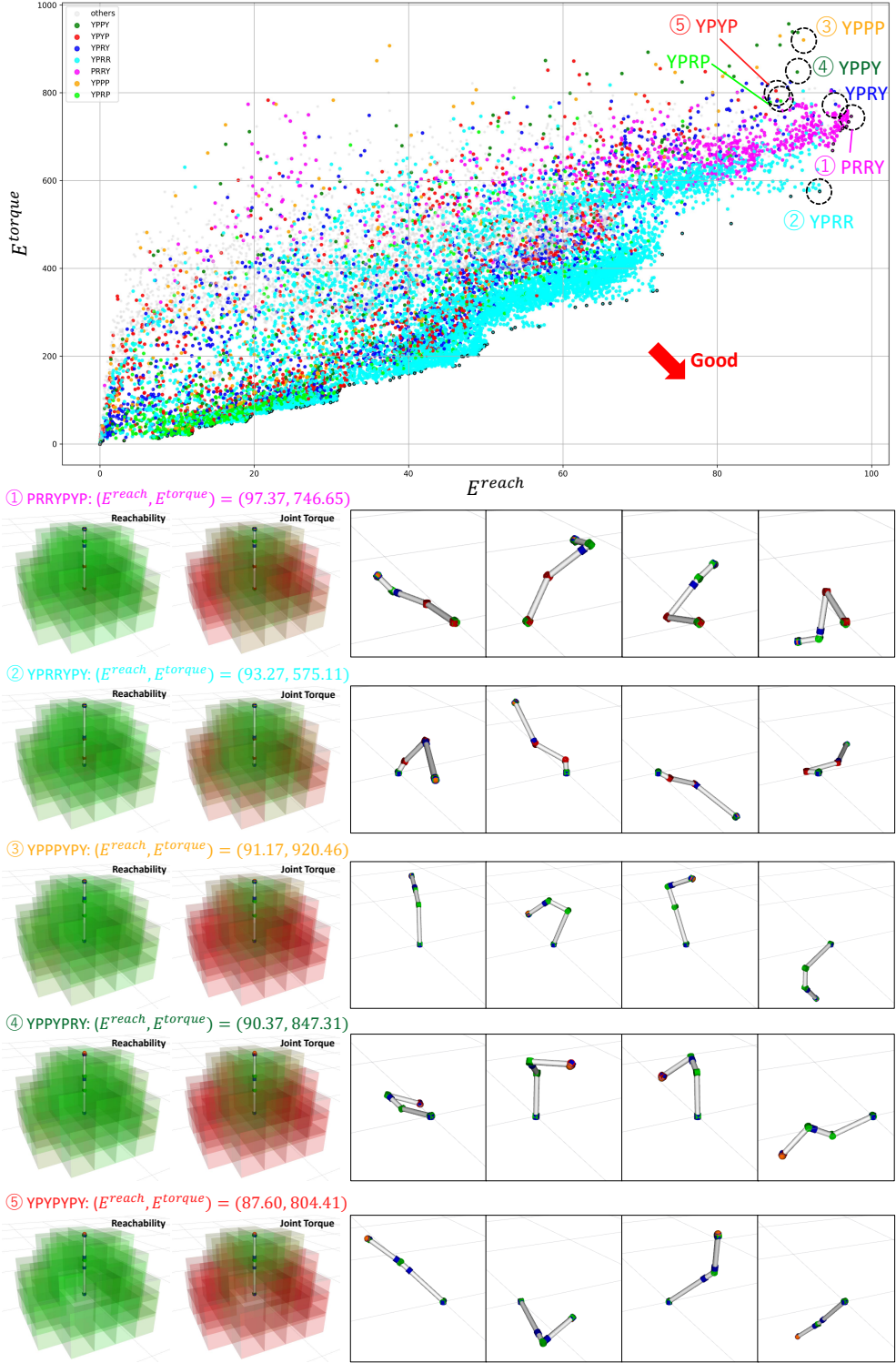


Figure 6. Optimization results for a 7-DOF manipulator: The upper figure visualizes the sampling results, color-coded based on differences in the first four joint types. The lower figure presents a subset of the solutions, showing end-effector reachability, joint torque, and four postures generated by assigning random joint angles.

the lower figure of Fig. 6. Additionally, the joint configurations with the highest reachability among the sampled non-Pareto-optimal solutions (YPPP, YPPY, and YPYP) are also presented.

Overall, the trends observed in the 7-DOF case are somewhat different from those in the 6-DOF case. While two degrees of freedom are concentrated near the origin (shoulder) and three degrees of freedom at the end-effector (wrist), as in the 6-DOF case, there are two distinct approaches for distributing the

remaining two degrees of freedom: one where they are grouped around the elbow, dividing the entire linkage into a 1:1 ratio, and another where they are distributed more evenly in a 1:1:1 ratio.

The specific joint configurations are discussed below. **PRRY** exhibits both high reachability and low required torque, consistent with the results from the 6-DOF case. As the degrees of freedom at the end-effector increase, reachability improves, but the required torque also increases. **YPRR** is a modification of the 6-DOF **PRRY** with an additional Yaw joint at the base. Since the first Yaw joint does not experience significant torque, the required torque remains nearly the same as in the 6-DOF **PRRY**, while reachability is improved. **YPPP**, **YPPY**, and **YPYP** have simple and intuitive joint structures, but as in the 6-DOF case, are more directly affected by gravitational effects. All three exhibit similar performance, but among them, **YPYP** has the lowest torque requirements. **YPYP** is one of the most common structures in industrial robots, and manipulators such as Franka Emika Panda, Sawyer, and Kinova Gen3 adopt similar configurations. Additionally, a robot with the **YPRP** structure is the Robai Cyton Gamma [29].

#### 4. Discussion

The obtained results are summarized and discussed below. First, regarding the trends in the sampling results, 6-DOF manipulators showed significant differences in joint structure performance, with distinct characteristics in terms of reachability and torque. In contrast, 7-DOF manipulators exhibited relatively high reachability across different joint structures, with no significant differences observed. This highlights the importance of joint configuration in 6-DOF manipulators. Additionally, while the link length ratios were generally similar among 6-DOF manipulators, greater variation was observed in the 7-DOF case.

Next, regarding specific joint configurations, many of the configurations found in the Pareto-optimal solutions were not commonly seen in real-world manipulators. In particular, the **PRRY** structure was found to have the highest reachability and the lowest torque for both 6-DOF and 7-DOF manipulators. This structure can be interpreted as a SCARA-type robot that moves horizontally, rotated using a Pitch joint. By concentrating the torque on the first Pitch joint and reducing the force applied to subsequent Roll joints, this configuration reduces the required torque by one Pitch joint compared to more conventional manipulators that connect to a YPP structure. In contrast, common manipulator structures such as **YPPP** and **YPPY** are more susceptible to gravitational effects but feature simple kinematics, making their motion intuitive and easy to understand. While high gear ratios in traditional robots have mitigated these issues, the advancement of low-gear-ratio direct-drive motors may accelerate demand for structures that further reduce the effects of gravity in the future.

In this study, multi-objective optimization was performed solely from the perspectives of end-effector reachability and joint torque. However, in reality, factors such as manufacturability and kinematic simplicity are also important. Considering these aspects to determine the most optimal structure would be highly meaningful. Rather than relying on human intuition, optimization based on data can provide interesting insights for future robot design. Additionally, another future challenge is determining the most optimal structure when incorporating not only rotational joints but also prismatic joints, closed-loop structures, and wire-driven mechanisms.

#### 5. Conclusion

In this study, a multi-objective optimization was performed from the perspectives of end-effector reachability and joint torque to analyze various manipulator structures. The design parameters consisted of discrete joint types and continuous link lengths, with additional constraints on joint sequences and total link length. A multi-objective optimization was efficiently conducted using the multivariate Tree-Structured Parzen Estimator (TPE). The optimization results revealed multiple novel manipulator structures that had not been previously explored while also clarifying the positions of existing manipulator structures within the optimization sampling. The differences in sampling results and Pareto-optimal solutions be-

tween 6-DOF and 7-DOF manipulators also provided interesting insights. Given the rapid advancements in motor technology, this study offers valuable guidance for future manipulator design. Of course, several interesting future challenges remain, such as the need to predefine certain parameters and the lack of consideration for kinematic simplicity or manufacturability. Nevertheless, this study provides a broad perspective on the performance of different joint structures.

## References

- [1] Jr George C Devol. Programmed article transfer, 1961. US Patent 2,988,237.
- [2] Tony Z. Zhao, Vikash Kumar, Sergey Levine, and Chelsea Finn. Learning Fine-Grained Bimanual Manipulation with Low-Cost Hardware. In *2023 Robotics: Science and Systems*, 2023.
- [3] R. Bommasani, et al. On the Opportunities and Risks of Foundation Models. arXiv preprint arXiv:2108.07258, 2021.
- [4] Roya Firoozi, Johnathan Tucker, Stephen Tian, Anirudha Majumdar, Jiankai Sun, Weiyu Liu, Yuke Zhu, Shuran Song, Ashish Kapoor, Karol Hausman, Brian Ichter, Danny Driess, et al. Foundation models in robotics: Applications, challenges, and the future. *The International Journal of Robotics Research*, 2024.
- [5] K. Kawaharazuka, T. Matsushima, A. Gambardella, J. Guo, C. Paxton, and A. Zeng. Real-World Robot Applications of Foundation Models: A Review. *Advanced Robotics*, 2024.
- [6] DENSO WAVE. COBOTTA Collaborative Robot. <https://www.denso-wave.com/en/robot/product/collabo/cobotta.html>. Accessed: 2025-02-28.
- [7] UFactory. xArm 6 Collaborative Robot. <https://www.ufactory.cc/xarm-collaborative-robot/>. Accessed: 2025-02-28.
- [8] Fangzhou Infinite. ARX Robot. <https://arx-x.com/>. Accessed: 2025-02-28.
- [9] Kevin Black, Noah Brown, Danny Driess, Adnan Esmail, Michael Equi, Chelsea Finn, Niccolò Fusai, Lachy Groom, Karol Hausman, Brian Ichter, et al. \pi\_0: A vision-language-action flow model for general robot control. *arXiv preprint arXiv:2410.24164*, 2024.
- [10] Elephant Robotics. myCobot 280 M5Stack. <https://www.elephantrobotics.com/en/mycobot-en/>. Accessed: 2025-02-28.
- [11] Franka Robotics. Franka Emika Panda. <https://franka.de/>. Accessed: 2025-02-28.
- [12] Rethink Robotics. Sawyer Collaborative Robot. <https://robotsguide.com/robots/sawyer>. Accessed: 2025-02-28.
- [13] Kinova Robotics. Kinova Gen3 Ultra-lightweight Robot. <https://www.kinovarobotics.com/product/gen3-robots>. Accessed: 2025-02-28.
- [14] B. Paden and S. Sastry. Optimal kinematic design of 6R manipulators. *The International Journal of Robotics Research*, Vol. 7, No. 2, pp. 43–61, 1988.
- [15] J. M. Hollerbach. Optimum kinematic design for a seven degree of freedom manipulator. In *Robotics research: The second international symposium*, pp. 215–222, 1985.
- [16] G. Yang and I. Chen. Task-based optimization of modular robot configurations: minimized degree-of-freedom approach. *Mechanism and Machine Theory*, Vol. 35, No. 4, pp. 517–540, 2000.
- [17] Y. Xiao, Z. Fan, W. Li, S. Chen, L. Zhao, and H. Xie. A Manipulator Design Optimization Based on Constrained Multi-objective Evolutionary Algorithms. In *2016 International Conference on Industrial Informatics*, pp. 199–205, 2016.
- [18] S. B. Liu and M. Althoff. Optimizing performance in automation through modular robots. In *2020 IEEE International Conference on Robotics and Automation*, pp. 4044–4050, 2020.
- [19] M. Lei, E. Romiti, A. Laurenz, and N. G. Tsagarakis. Task-Driven Computational Framework for Simultaneously Optimizing Design and Mounted Pose of Modular Reconfigurable Manipulators. In *2024 IEEE/RSJ International Conference on Intelligent Robots and Systems*, 2024.
- [20] K. Kawaharazuka, T. Makabe, K. Okada, and M. Inaba. Daily Assistive Modular Robot Design Based on Multi-Objective Black-Box Optimization. In *2023 IEEE/RSJ International Conference on Intelligent Robots and Systems*, pp. 9970–9977, 2023.
- [21] K. Kawaharazuka, K. Okada, and M. Inaba. Robot Design Optimization with Rotational and Prismatic Joints Using Black-Box Multi-Objective Optimization. In *2024 IEEE/RSJ International Conference on Intelligent Robots and Systems*, pp. 4571–4577, 2024.
- [22] J. S. Bergstra, R. Bardenet, Y. Bengio, and B. Kégl. Algorithms for Hyper-Parameter Optimization. In *2011 Neural Information Processing Systems*, pp. 2546–2554, 2011.

- [23] F. Zacharias, C. Borst, and G. Hirzinger. Capturing robot workspace structure: representing robot capabilities. In *2007 IEEE/RSJ International Conference on Intelligent Robots and Systems*, pp. 3229–3236, 2007.
- [24] T. F. Chan and R. V. Dubey. A weighted least-norm solution based scheme for avoiding joint limits for redundant joint manipulators. *IEEE Transactions on Robotics and Automation*, Vol. 11, No. 2, pp. 286–292, 1995.
- [25] H. Sugiura, M. Gienger, H. Janssen, and C. Goerick. Real-time collision avoidance with whole body motion control for humanoid robots. In *2007 IEEE/RSJ International Conference on Intelligent Robots and Systems*, pp. 2053–2058, 2007.
- [26] S. Falkner, A. Klein, and F. Hutter. BOHB: Robust and efficient hyperparameter optimization at scale. In *35th International Conference on Machine Learning*, pp. 1437–1446, 2018.
- [27] T. Akiba, S. Sano, T. Yanase, T. Ohta, and M. Koyama. Optuna: A Next-generation Hyperparameter Optimization Framework. In *25th ACM SIGKDD International Conference on Knowledge Discovery and Data Mining*, 2019.
- [28] Boston Dynamics. Spot Robot. <https://www.bostondynamics.com/spot>. Accessed: 2025-02-28.
- [29] Robai. Cyton Gamma 1500 Robotic Arm. <https://www.cdiweb.com/datasheets/robai/cyton-gamma-1500-brochure.pdf>. Accessed: 2025-02-28.